

Different Dynamic Formulations for a Mechanism using Bond Graph

Aman Kumar MAINI*, Anand VAZ

*Department of Mechanical Engineering
Dr. B. R. Ambedkar National Institute of Technology*

Jalandhar – 144011, Punjab, India

e-mail: anandvaz@ieee.org

*Corresponding Author e-mail: amanmaini1975@gmail.com

For modeling dynamics of mechanisms, various classical formulations are available in the literature. The equations of dynamics given by various classical formulations can also be derived from the bond graph. The bond graph is a convenient graphical representation for modeling dynamics of physical systems in multi-energy domains.

In this paper, various alternative causality assignment procedures in the bond graph are used to derive different classical formulations such as the Lagrange's equations of the first kind (with λ multipliers), Lagrange's formulation of the second kind, and Hamiltonian formulations. An example of the quick return mechanism has been modeled using the bond graph technique, and various alternative causality assignment procedures are applied to derive the various formulations. Simulation coding has been done using MATLAB and results have been analyzed and discussed. The purpose of this paper is to show how the various formulations can be obtained from bond graph using various alternative causality assignment procedures.

Keywords: bond graph, classical formulations, modeling, system dynamics.

1. INTRODUCTION

For dynamics of mechanisms, various classical formulations like the Newton-Euler, Lagrange's and Hamilton's formulations are found in several references [1–3]. The energy-based formulations, commonly used for modeling dynamics of physical systems, usually tend to be too mathematically inclined and cumbersome for large multibody systems.

The bond graph technique introduced by Professor Henry Paynter in 1959, is the graphical representation of a physical system's dynamics. The bond graph is computationally advantageous for dynamic analysis of mechanisms and espe-

cially convenient for modeling of physical system dynamics in multiple energy domains [4–11]. A well-known advantage of bond graph models is that they can be manipulated manually to obtain first-order state equations. In addition, a simple description of causality in the bond graph shows the *cause* and *effect* relationship between the flow and effort variables of the power bond [7–10]. The equations representing the dynamics of a system can be derived algorithmically from the bond graph model. This approach offers a greater scope for analysis of causality, an important aspect of physical systems, and a feature not offered by the energy-based formulations.

The equations of dynamics, given by various classical formulations such as Lagrange's and Hamilton's formulations, can also be derived from the bond graph using various causality assignment procedures [12]. These causality assignment procedures are the sequential causality assignment procedure (SCAP), the Lagrangian causality assignment procedure (LCAP), and the relaxed causality assignment procedure (RCAP). Alternative causality assignment procedures such as LaCAP for obtaining the Lagrange equations, HaCAP for the Hamilton equations, and BHCAP for obtaining the Boltzmann-Hamel equations are also proposed in the literature [12].

In this paper, the procedure to derive different classical formulations using various causality assignment procedures in the bond graph is explored. An example of a quick return mechanism has been modeled using the bond graph technique. Various causality assignment procedures are applied to derive different formulations. In the quick return mechanism, sliding and turning motions act simultaneously; hence, the Coriolis component of acceleration comes into the picture. This mechanism has been selected intentionally for modeling. The Lagrange's equation of the first kind with the Lagrange multiplier λ , Lagrange's equation of the second kind, and Hamilton's formulations have been derived algorithmically from the bond graph model based on the causal information propagation. However, coding for simulation has been done directly from the bond graph. Program coding is implemented using MATLAB. Important kinematic and dynamic quantities have been plotted, analyzed, and explained. The results from both formulations are compared and discussed.

The paper is organized as follows. Modeling of a quick return mechanism is explained in the next section. Section 3 describes the procedure for derivation of the Lagrangian formulation of the first kind with λ multiplier from the bond graph using the causality assignment procedure. The procedure for obtaining the Lagrangian formulation of the second kind is discussed in Sec. 4. Section 5 explains the derivation of Hamiltonian formulation from the bond graph. Simulation and results are analyzed and discussed in Sec. 6. Section 7 presents the conclusion and discussion.

2. MODELING OF A QUICK RETURN MECHANISM

The quick return mechanism, used in the shaper and slotting machines in industries, is a well-known mechanism. The schematic diagram of a quick return mechanism is shown in Fig. 1.

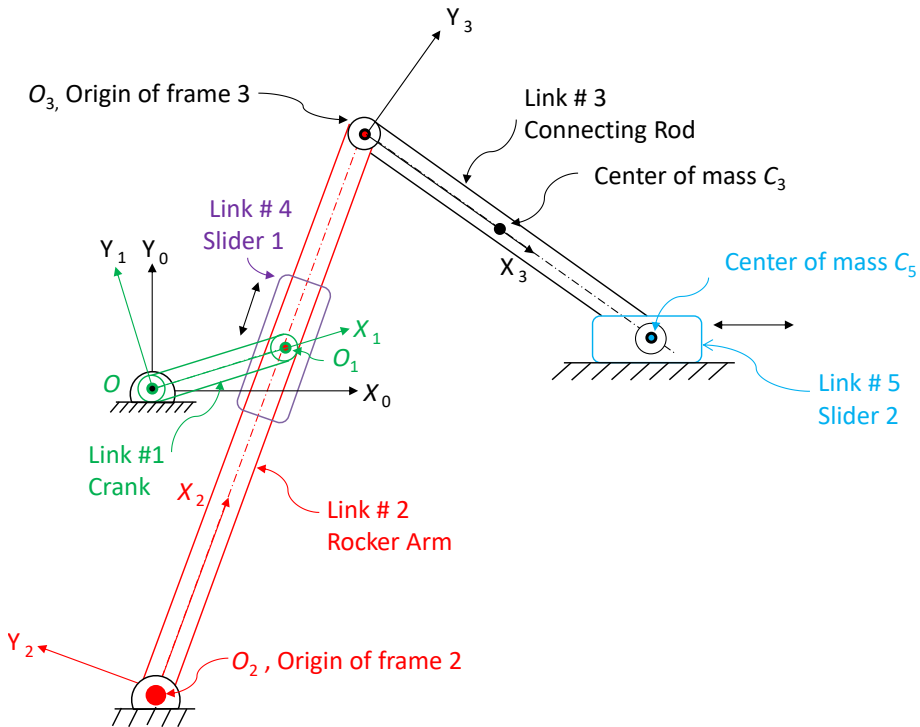


FIG. 1. Diagram of a quick return mechanism.

It consists of five rigid links interconnected to each other by revolute as well as prismatic joints. Frame $\{0\}$, which is a fixed frame, is considered as an inertial frame. The origins of the frame $\{0\}$ and the frame $\{1\}$ coincide with each other at point O .

The mechanism involves link 1 as the crank, which rotates about its origin O , and another end of the crank is connected to link 4 (slider 1) by a pin joint at point O_1 . Frame $\{2\}$ is fixed on the rocker arm (link 2). Point O_2 is the origin of the rocker arm. The rocker arm oscillates about its origin O_2 .

The second end of the rocker arm is connected to the connecting rod (link 3) at point O_3 using a pin joint. Point O_3 is the origin of the frame fixed on link 3. The connecting rod transmits the movement to link 5 (slider 2), which reciprocates horizontally, as shown in Fig. 1.

The center of mass of each link is assumed to be located at the geometrical center of the link, C_3 and C_5 are the centers of masses of link 3 and link 5, respectively. Figure 2 shows the initial geometrical posture of the quick return mechanism. Dimension “h”, shown in Fig. 2, is the vertical gap between the origin of the frame $\{1\}$ and the origin of the frame $\{2\}$, while “H” is the vertical distance between the origin O_2 and the slider 2.

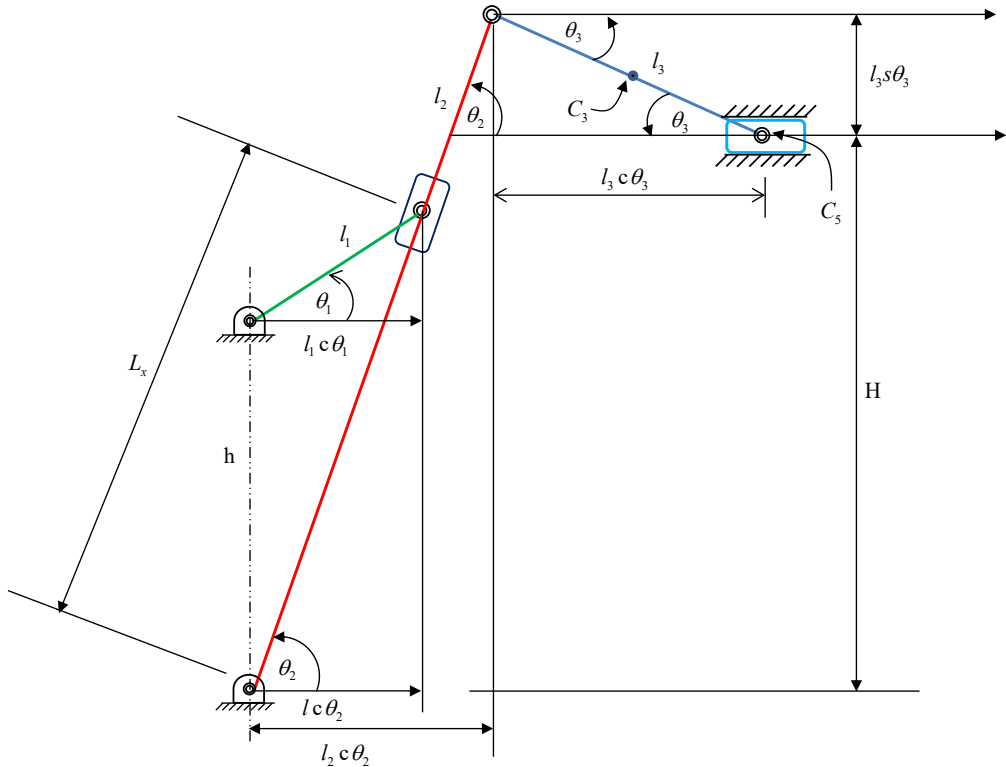


FIG. 2. The initial geometrical posture of the quick return mechanism.

The angle between the crank and the inertial frame is considered as θ_1 . The angle θ_2 represents the initial angular position of the rocker arm. The angle between the connecting rod and a line parallel to the inertial frame is represented by θ_3 . Table 1 shows the various link properties considered in the bond graph modeling of the mechanism.

Considering a planar case, in Fig. 3, \dot{x}_{C_3} and \dot{y}_{C_3} represent X -component and Y -component of the translational velocities of the center of mass C_3 while these components of C_5 are represented by \dot{x}_{C_5} and \dot{y}_{C_5} , respectively.

These translational velocities are represented by 1-junctions: $1_{\dot{x}_{C_3}}$, $1_{\dot{y}_{C_3}}$ and $1_{\dot{x}_{C_5}}$, $1_{\dot{y}_{C_5}}$, respectively. Rotational velocities, $\dot{\theta}_1$ of the crank, $\dot{\theta}_2$ of the rocker

arm and $\dot{\theta}_3$ of the connecting rod are represented by the junctions $1_{\dot{\theta}_1}$, $1_{\dot{\theta}_2}$ and $1_{\dot{\theta}_3}$, respectively.

TABLE 1. Link properties used for simulation (ref. Figs 1 and 2).

Crank (Link 1)		
${}^1l_x = 0.08 \text{ m}$	${}^1l_y = 0.01 \text{ m}$	${}^1l_z = 0.01 \text{ m}$
Link 2		
${}^2l_x = 0.8 \text{ m}$	${}^2l_y = 0.01 \text{ m}$	${}^2l_z = 0.01 \text{ m}$
Link 3		
${}^3l_x = 1.0 \text{ m}$	${}^3l_y = 0.01 \text{ m}$	${}^3l_z = 0.01 \text{ m}$
Vertical distance between the slider and origin of frame $\{2\}$		
$H = 0.55 \text{ m}$		
Vertical distance between the inertial frame and frame $\{2\}$		
$h = 0.35 \text{ m}$		
The angle between link 1 and inertial frame		
θ_1		
The angle between link 2 and inertial frame		
θ_2		
The angle between link 3 and inertial frame		
θ_3		
$c\theta = \cos \theta$ while $s\theta = \sin \theta$		

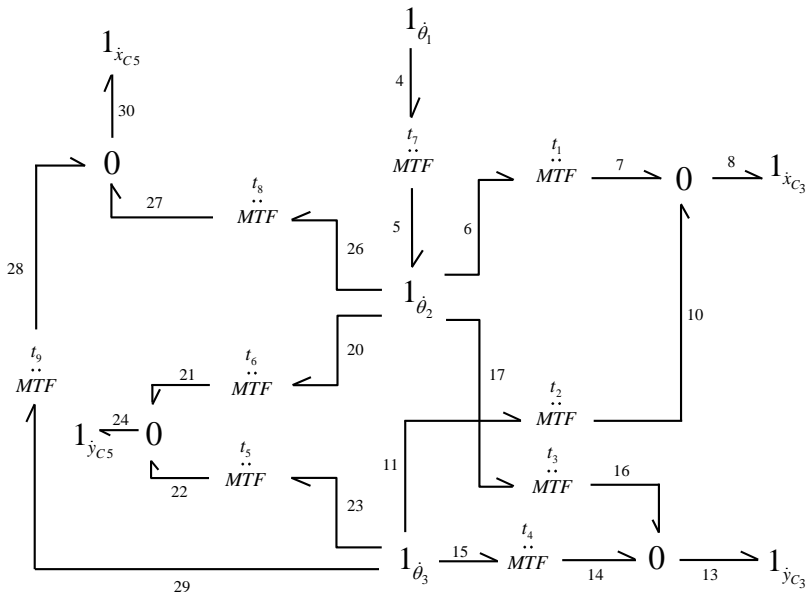


FIG. 3. Bond graph showing the kinematics of the quick return mechanism.

The kinematics relationship among the various links, evaluated based on Fig. 2, is given below:

Position of the center of mass C_3 of link 3 (X -component):

$$x_{C_3} = l_2 c \theta_2 + l_{C_3} c \theta_3; \quad (1)$$

Velocity of the center of mass C_3 of link 3 (X -component):

$$\dot{x}_{C_3} = -l_2 s \theta_2 \dot{\theta}_2 - l_{C_3} s \theta_3 \dot{\theta}_3; \quad (2)$$

Position of the center of mass C_3 of link 3 (Y -component):

$$y_{C_3} = l_2 s \theta_2 - l_{C_3} s \theta_3; \quad (3)$$

Velocity of the center of mass C_3 of link 3 (Y -component):

$$\dot{y}_{C_3} = l_2 c \theta_2 \dot{\theta}_2 - l_{C_3} c \theta_3 \dot{\theta}_3; \quad (4)$$

Position of the center of mass C_5 of link 5 (X -component):

$$x_{C_5} = l_2 c \theta_2 + l_3 c \theta_3; \quad (5)$$

Velocity of the center of mass C_5 of link 5 (X -component):

$$\dot{x}_{C_5} = -l_2 s \theta_2 \dot{\theta}_2 - l_3 s \theta_3 \dot{\theta}_3, \quad (6)$$

$$\dot{x}_{C_5} = -l_2 s \theta_2 (l_1 c (\theta_2 - \theta_1)) \dot{\theta}_1 - l_3 s \theta_3 \dot{\theta}_3; \quad (7)$$

Position of the center of mass C_5 of link 5 (Y -component):

$$y_{C_5} = l_2 s \theta_2 - l_3 s \theta_3; \quad (8)$$

Velocity of the center of mass C_5 of link 5 (Y -component):

$$\dot{y}_{C_5} = l_2 c \theta_2 \dot{\theta}_2 - l_3 c \theta_3 \dot{\theta}_3 = 0. \quad (9)$$

The kinematic relationships between the translational velocities of the center of masses C_3 and C_5 , and the rotational velocities of link 1, link 2, and link 3 are represented by Eqs (1) to (9). These translational velocities and the rotational velocities are related using modulated transformers (MTFs): t_i , where $i = 1$ to 9. The values of these MTFs are shown in Table 2. These values have been calculated based on the kinematic relationships between the various links of the mechanism (shown in Fig. 2).

Each mechanism consists of several rigid links interconnected with the help of various types of joints. The dynamics of a rigid body consists of translational

TABLE 2. Various modulated transformers (MTFs) used in bond graph.

Modulated transformers (MTFs)	Value
t_1	$-l_2 S \theta_2$
t_2	$-l_{G_3} S \theta_3$
t_3	$l_2 C \theta_2$
t_4	$-l_{G_3} C \theta_3$
t_5	$-l_3 C \theta_3$
t_6	$l_2 C \theta_2$
t_7	$l_1 C (\theta_2 - \theta_1) / l_x$
t_8	$-l_2 S \theta_2$
t_9	$-l_3 S \theta_3$

as well as rotational part. During bond graph modeling of a mechanism, the modeling of each rigid link is initiated using its kinematics based on the flow mapping approach. When the mass of the link is considered, the translational and the rotational dynamics come into the picture, and this is shown in the bond graph structure in Fig. 5, and their effects are just appended to the bond graph of the previous kinematic structure, shown in Fig. 4. This is the beautiful feature of the bond graph technique.

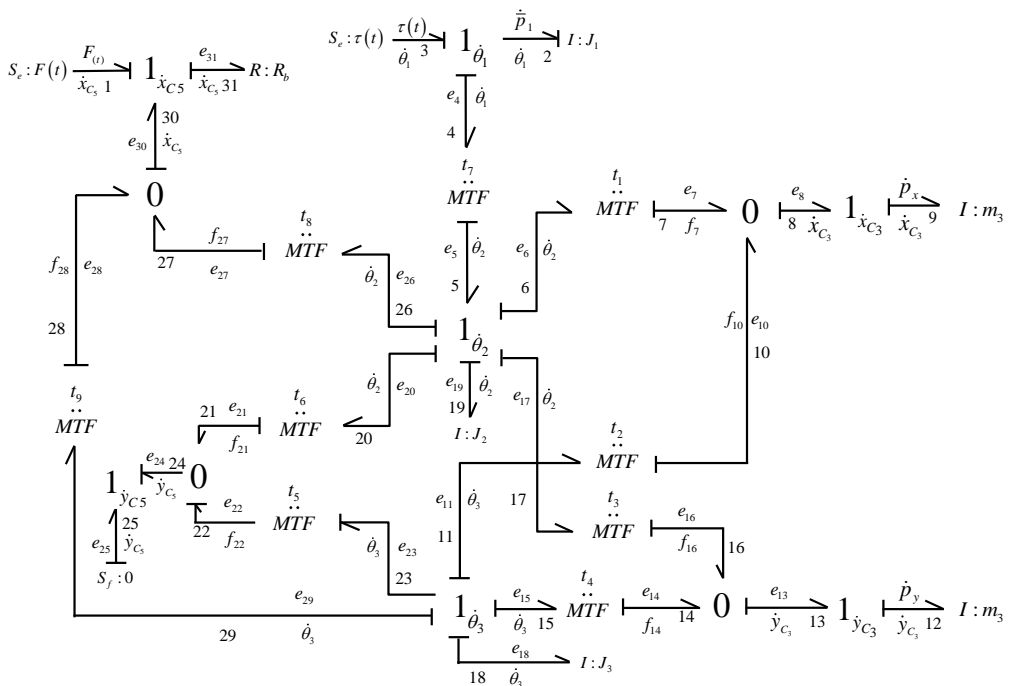


FIG. 4. Bond graph of the quick return mechanism.

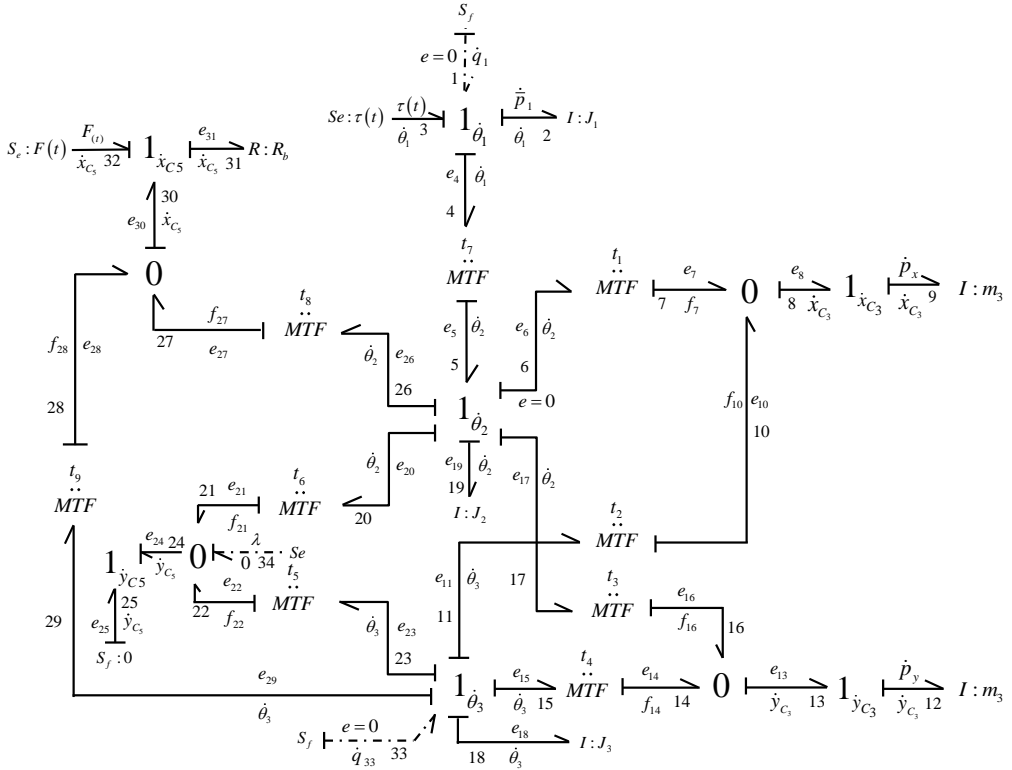


FIG. 5. Bond graph of the system with the Lagrange multiplier.

In the bond graph, shown in Fig. 4, the translational momentum of link 3 has been considered to be concentrated at the center of mass C_3 . The mass of link 3 is taken as m_3 . The translational inertia $I: m_3$ of link 3 is connected by bond 9 at the junction $1_{\dot{x}_{C_3}}$ and by bond 12 at the junction $1_{\dot{y}_{C_3}}$, respectively. The torque $\tau(t)$ applied at the crank is represented by the source of effort $S_e: \tau(t)$ by the bond 3. The rotational inertia $I: J_1$ of link 1, $I: J_2$ of link 2, and $I: J_3$ of link 3 are attached at the junction $1_{\dot{\theta}_1}$ by bond 2, $1_{\dot{\theta}_2}$ by bond 19 and at $1_{\dot{\theta}_3}$ by bond 18, respectively.

3. DERIVATION OF THE LAGRANGIAN FORMULATION OF THE FIRST KIND FROM THE BOND GRAPH

The standard form of Lagrange's equation for a system having generalized displacements $q_1, q_2, q_3, \dots, q_n$ and their rates of changes $\dot{q}_1, \dot{q}_2, \dot{q}_3, \dots, \dot{q}_n$ is:

$$\frac{d}{dt} \frac{\partial L}{\partial \dot{q}_i} - \frac{\partial L}{\partial q_i} = E_i, \quad i = 1, 2, 3, \dots, n, \tag{10}$$

where the Lagrangian formulation is:

$$L(q_1, q_2, \dots, q_n, \dot{q}_1, \dot{q}_2, \dots, \dot{q}_n, t) \quad \text{is} \quad (11)$$

$$L = T^*(q_1, q_2, \dots, q_n, \dot{q}_1, \dot{q}_2, \dots, \dot{q}_n, t) - V(q_1, q_2, \dots, q_n, t).$$

T^* and V are respectively the sums of the all kinetic co-energies and the potential energies in the system, and the quantities E_i are generalized forces for the i -th coordinates. For mechanical systems, the difference between kinetic energy and kinetic co-energy is not important because the Newtonian mass law is linear, and numerically kinetic energy and kinetic co-energy are equal. For other energy domains, this distinction is important. This distinction is crucial for nonlinear systems and in any case, T^* is properly a function of \dot{q}_i [3]. Since the Lagrangian method and the bond graph method are based on power and energy interactions, there should be some connection between these two techniques. The state functions associated with I -elements and C -elements can be used to derive the standard Lagrange equation. Potential energies are associated with C -elements, while kinetic energies are associated with I -elements. The state functions required to derive Lagrange's equation from the bond graph are explained by Karnopp [13] and Brown [14].

The bond graph model of the quick return mechanism is shown in Fig. 5. The Lagrange formulation of the first kind with the Lagrange multiplier λ can be obtained from the bond graph using the causality assignment procedure, as shown in Fig. 5.

To obtain a Lagrange multiplier, attach an artificial source of flow (ASF) to the generalized 1-junctions. Generalized 1-junction is a 1-junction to which a generalized velocity is attached and where a Lagrange equation will be expressed by an effort balance. The flow imposed by this source is a generalized velocity, and the corresponding effort is equal to zero. The causality of the bond graph structure of the system is propagated starting from ASF [12].

If the causal conflicts appear at any 0-junction then connect an artificial effort source (AES) to the 0-junctions, they are then called constrained 0-junction. A constrained 0-junction is an 0-junction to which a Lagrange multiplier λ is attached and where an equation will be expressed in its kinematic form by a flow balance. The effort imposed by the source is the Lagrange multiplier λ and the corresponding flow is equal to zero. The equation obtained (33) from the bond graph will be in terms of λ (Lagrange multiplier) [12].

In Fig. 5, the torque $S_e : \tau(t)$ applied at the crank is attached by bond 3 at the junction $1_{\dot{\theta}_1}$. An ASF (S_f ; shown by a dotted line) is attached at the junction $1_{\dot{\theta}_1}$ by bond 1, which imposes flow \dot{q}_1 to which corresponding effort e_1 is zero. This flow information is propagated into the junction structure. An artificial flow of source attached to each common flow junctions $1_{\dot{\theta}_1}$ and $1_{\dot{\theta}_3}$ represents

the time derivative of the generalized displacement q_1 and q_{33} , respectively. Generalized force \dot{p}_1 is the effort into the artificial source of flow at that common flow junction $1_{\dot{\theta}_1}$. The flow \dot{q}_1 has been transmitted through an MTF: t_7 to the rest of the elements. At the junction $1_{\dot{\theta}_2}$, the flow $\dot{\theta}_2$ comes from bond 5 and it is transmitted to the center of masses of link 3 and link 5. The velocity \dot{Y}_{C_5} is constrained by $S_f: 0$ at bond 25 because the movement of the slider 2 (in Fig. 1) is permitted in one direction only.

From the bond graph shown in Fig. 5, the Lagrange equation of the first kind can be derived using the following procedure:

$$e_1 = 0 = e_2 + e_4 - e_3, \quad (12)$$

$$e_1 = J_1\ddot{\theta}_1 + t_7e_5 - \tau(t), \quad (13)$$

$$e_1 = J_1\ddot{\theta}_1 + t_7[e_6 + e_{17} + e_{19} + e_{20} + e_{26}] - \tau(t), \quad (14)$$

$$e_1 = J_1\ddot{\theta}_1 + t_7t_1e_7 + t_7t_3e_{16} + t_7J_2\ddot{\theta}_2 + t_7t_6e_{21} + t_7t_8e_{27} - \tau(t), \quad (15)$$

$$e_1 = J_1\ddot{\theta}_1 + t_7t_1e_8 + t_7t_3e_{13} + t_7J_2\ddot{\theta}_2 + t_7t_6\lambda + t_7t_8e_{30} - \tau(t), \quad (16)$$

$$e_1 = J_1\ddot{\theta}_1 + t_7t_1\dot{p}_x + t_7t_3\dot{p}_y + t_7J_2\ddot{\theta}_2 + t_7t_6\lambda + t_7t_8(e_{31} - e_{32}) - \tau(t), \quad (17)$$

$$e_1 = J_1\ddot{\theta}_1 + t_7t_1\dot{p}_x + t_7t_3\dot{p}_y + t_7J_2\ddot{\theta}_2 + t_7t_6\lambda + t_7t_8(Rf_{31} - F(t)) - \tau(t). \quad (18)$$

Value p_x can be calculated in terms of $\dot{\theta}_1$:

$$p_x = m \left(t_1t_7\dot{\theta}_1 - \frac{t_2t_6t_7}{t_5}\dot{\theta}_1 \right), \quad (19)$$

$$e_8 = \dot{p}_x = m \frac{d}{dt} \left(t_1t_7\dot{\theta}_1 - \frac{t_2t_6t_7}{t_5}\dot{\theta}_1 \right), \quad (20)$$

$$\dot{p}_x = e_8 = m \frac{d}{dt} \left(t_1t_7\dot{\theta}_1 \right) - m \frac{d}{dt} \left(\frac{t_2t_6t_7}{t_5}\dot{\theta}_1 \right), \quad (21)$$

$$\begin{aligned} \dot{p}_x = m & \left[t_1t_7\ddot{\theta}_1 + \dot{\theta}_1t_1\dot{t}_7 + \dot{\theta}_1t_7\dot{t}_1 \right] \\ & - m \left(\frac{t_5 \frac{d}{dt} \left(t_2t_6t_7\dot{\theta}_1 \right) - t_2t_6t_7\dot{\theta}_1 \frac{d}{dt} (t_5)}{(t_5)^2} \right), \quad (22) \end{aligned}$$

$$\dot{p}_x = m \left[t_1 t_7 \ddot{\theta}_1 + \dot{\theta}_1 t_1 \dot{t}_7 + \dot{\theta}_1 t_7 \dot{t}_1 \right] - m \left(\frac{t_6 t_7 \dot{\theta}_1 d(t_2)}{t_5} + \frac{t_2 t_7 \dot{\theta}_1 d(t_6)}{t_5} \right. \\ \left. + \frac{t_2 t_6 \dot{\theta}_1 d(t_7)}{t_5} + \frac{t_2 t_6 t_7 d(\ddot{\theta}_1)}{t_5} - \frac{t_2 t_6 t_7 \dot{\theta}_1 d(t_5)}{(t_5)^2} \right), \quad (23)$$

$$J_2 \ddot{\theta}_2 = J_2 \frac{d(t_7 \dot{\theta}_1)}{dt} = J_2 \dot{\theta}_1 \dot{t}_7 + J_2 t_7 \ddot{\theta}_1. \quad (24)$$

Value \dot{p}_y can be calculated in terms of $\dot{\theta}_1$:

$$p_y = m f_{12} = m f_{13} = m (f_{16} + f_{14}), \quad (25)$$

$$m (t_3 f_{17} + t_4 f_{15}) = m (t_3 t_7 \dot{\theta}_1 + t_4 f_{23}) = m (t_3 t_7 \dot{\theta}_1 - t_4 f_{21}) \quad (26)$$

$$= m (t_3 t_7 \dot{\theta}_1 - t_4 t_6 t_7 \dot{\theta}_1), \quad (27)$$

$$e_{13} = \dot{p}_y = \frac{d \left[m (t_3 t_7 \dot{\theta}_1 - t_4 t_6 t_7 \dot{\theta}_1) \right]}{dt}. \quad (28)$$

Simplifying Eq. (28),

$$\dot{p}_y = m t_3 t_7 \ddot{\theta}_1 + m t_3 \dot{t}_7 \dot{\theta}_1 + m t_7 \dot{t}_3 \dot{\theta}_1 \\ - m t_4 t_6 t_7 \ddot{\theta}_1 - m t_4 t_6 \dot{t}_7 \dot{\theta}_1 - m t_6 t_7 \dot{t}_4 \dot{\theta}_1 - m t_4 t_7 \dot{t}_6 \dot{\theta}_1, \quad (29)$$

$$e_{30} = e_{31} - e_{32} = R f_{31} - F(t). \quad (30)$$

Simplifying Eq. (30),

$$e_{30} = R \left[- \left(\frac{t_9}{t_5} \right) t_6 t_7 \dot{\theta}_1 + t_8 t_7 \dot{\theta}_1 \right] - F(t). \quad (31)$$

By putting the values of p_x , p_y , J_2 , $\ddot{\theta}_2$ and $Rf_{31} - F(t)$ in Eq. (18), one can obtain the main equations given below by Eqs (32), (33) and (34):

$$\begin{aligned} & \left(J_1 + m(t_1 t_7)^2 - \frac{m(t_7)^2 t_1 t_2 t_6}{t_5} + J_2(t_7)^2 + m(t_3 t_7)^2 - m t_4 t_6 (t_7)^2 t_3 \right) \ddot{q}_1 \\ & + \left(m(t_1)^2 t_7 \dot{t}_7 + m t_1 (t_7)^2 \dot{t}_1 - \frac{m(t_7)^2 t_1 t_6 \dot{t}_2}{t_5} - \frac{m t (t_7)^2 t_1 t_2 \dot{t}_6}{t_5} \right. \\ & \quad - \frac{m t_7 t_1 t_2 t_6 \dot{t}_7}{t_5} + \frac{m(t_7)^2 t_1 t_2 t_6 \dot{t}_5}{(t_5)^2} + J_2 t_7 \dot{t}_7 + m(t_3)^2 t_7 \dot{t}_7 \\ & \quad + m t_3 (t_7)^2 \dot{t}_3 - m t_3 t_7 t_4 t_6 \dot{t}_7 - m t_4 t_3 (t_7)^2 \dot{t}_6 - m t_6 t_3 (t_7)^2 \dot{t}_4 \\ & \quad \left. - R \frac{t_9 t_8 (t_7)^2 t_6}{t_5} + R(t_7 t_8)^2 \right) \dot{q}_1 + t_7 t_6 \lambda - (t_7 t_8) F - \tau(t) = 0, \quad (32) \end{aligned}$$

$$\begin{aligned} & \left(\frac{J_3 t_6 t_7}{t_5} + m t_4 t_3 t_7 - m t_6 t_7 (t_4)^2 + m t_1 t_7 t_2 - \frac{m(t_2)^2 t_7 t_6}{t_5} \right) \ddot{q}_1 \\ & + \left(\frac{J_3 t_7 \dot{t}_6}{t_5} + \frac{J_3 t_6 \dot{t}_7}{t_5} - \frac{J_3 t_6 t_7 \dot{t}_5}{(t_5)^2} + m t_3 t_4 \dot{t}_7 + m t_7 t_4 \dot{t}_3 \right. \\ & \quad - m(t_4)^2 t_6 \dot{t}_7 - m(t_4)^2 t_7 \dot{t}_6 - m t_4 t_7 t_6 \dot{t}_4 + m t_1 t_2 \dot{t}_7 + m t_7 t_2 \dot{t}_1 \\ & \quad - \frac{m t_7 t_2 t_6 \dot{t}_2}{t_5} - \frac{m(t_2)^2 t_7 \dot{t}_6}{t_5} - \frac{m(t_2)^2 t_6 \dot{t}_7}{t_5} - \frac{m(t_2)^2 t_6 t_7 \dot{t}_5}{(t_5)^2} \\ & \quad \left. - \frac{R t_6 t_7 (t_9)^2}{t_5} + R t_9 t_8 t_7 \right) \dot{q}_1 + t_5 \lambda - t_9 F(t) = 0, \quad (33) \end{aligned}$$

$$t_6 t_7 \dot{q}_1 + t_5 \dot{q}_{33} = 0. \quad (34)$$

Equations (32), (33) and (34) represent the Lagrange formulation of the first kind. If the λ multiplier is eliminated using Eqs (32) and (33), the remaining equation will be the same as (35) given by the Lagrangian formulation of the second kind.

4. DERIVATION OF THE LAGRANGIAN FORMULATION OF THE SECOND KIND FROM THE BOND GRAPH

To obtain the Lagrange formulation of the second kind, an ASF is attached at the junction $1_{\dot{\theta}_1}$ by bond 1, as shown in Fig. 6. The ASF imposes flow \dot{q}_1 to which corresponding effort e_1 is zero. In the bond graph, I -element attached by bond 2 is in derivative causality. This means the system has a single degree of freedom with general displacement $q_1 = \theta_1$.

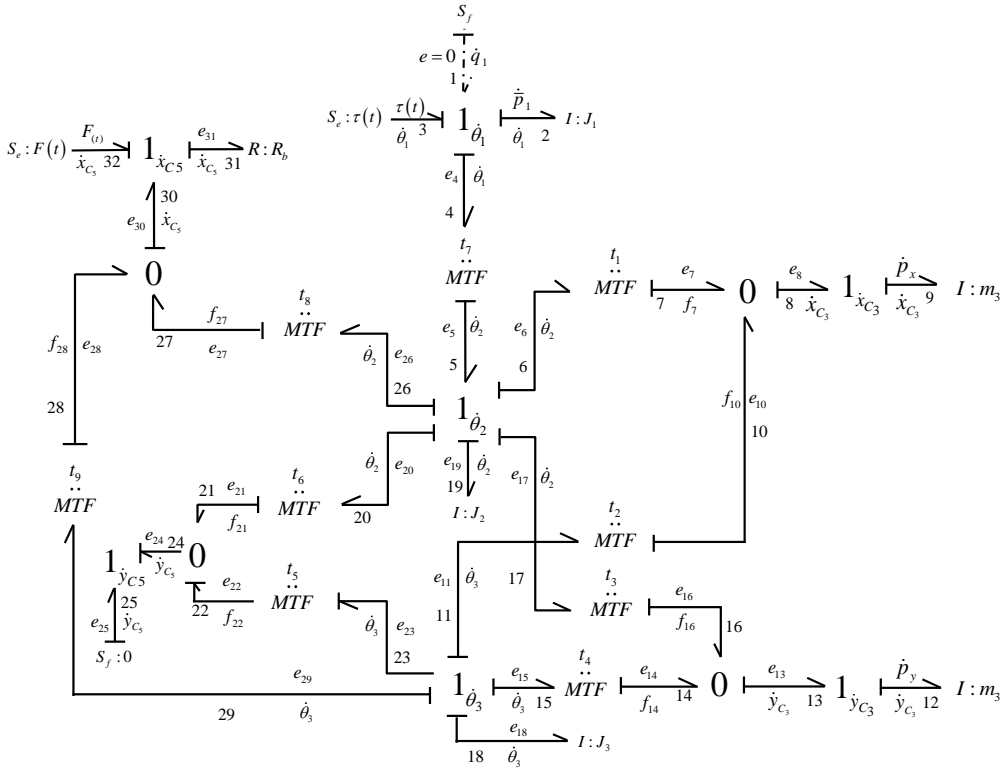


FIG. 6. Bond graph of the Lagrange formulation of the second kind.

The equation of dynamics can be derived from the bond graph algorithmically as mentioned above in Sec. 3. Obtained Eq. (35) is Lagrange’s equation of the second kind.

The Lagrange equation of quick return mechanism:

$$\ddot{q}_1 = \frac{-(a^*)\dot{q}_1 - \left(\frac{t_9 t_7 t_6}{t_5} - t_7 t_8\right) F + \tau}{b^*}, \tag{35}$$

where

$$\begin{aligned}
a^* = & m(t_1)^2 t_7 \dot{t}_7 + m t_1 (t_7)^2 \dot{t}_1 - \frac{m(t_7)^2 t_1 t_6}{t_5} \dot{t}_2 - \frac{m(t_7)^2 t_1 t_2}{t_5} \dot{t}_6 - \frac{m t_7 t_1 t_2 t_6}{t_5} \dot{t}_7 \\
& + \frac{m(t_7)^2 t_1 t_2 t_6}{(t_5)^2} \dot{t}_5 + J_2 t_7 \dot{t}_7 + m (t_3)^2 t_7 \dot{t}_7 + m t_3 (t_7)^2 \dot{t}_3 - m t_3 t_7 t_4 t_6 \dot{t}_7 \\
& - m t_4 t_3 (t_7)^2 \dot{t}_6 - m t_6 t_3 (t_7)^2 \dot{t}_4 - \frac{m t_2 t_1 t_7 t_6}{t_5} \dot{t}_7 - \frac{m t_2 (t_7)^2 t_6}{t_5} \dot{t}_1 \\
& + m t_2 \left(\frac{t_7 t_6}{t_5} \right)^2 \dot{t}_2 + m t_6 \left(\frac{t_7 t_2}{t_5} \right)^2 \dot{t}_6 + m t_7 \left(\frac{t_2 t_6}{t_5} \right)^2 \dot{t}_7 + m \frac{(t_2 t_6 t_7)^2}{(t_5)^3} \dot{t}_5 \\
& - \frac{m t_4 t_3 t_7 t_6}{t_5} \dot{t}_7 - \frac{m t_4 (t_7)^2 t_6}{t_5} \dot{t}_3 + \frac{m (t_4 t_6)^2 t_7}{t_5} \dot{t}_7 + \frac{m (t_4 t_7)^2 t_6}{t_5} \dot{t}_6 \\
& + \frac{m t_4 (t_6 t_7)^2}{t_5} \dot{t}_4 + \frac{J_3 t_6 (t_7)^2}{(t_5)^2} \dot{t}_6 + \frac{J_3 t_7 (t_6)^2}{(t_5)^2} \dot{t}_7 - \frac{J_3 (t_6 t_7)^2}{(t_5)^3} \dot{t}_5 \\
& + R \left(\frac{t_6 t_7 t_9}{t_5} \right)^2 - 2R \frac{t_9 t_8 (t_7)^2 t_6}{t_5} + R (t_7 t_8)^2,
\end{aligned}$$

$$\begin{aligned}
b^* = & J_1 + m (t_1 t_7)^2 - \frac{m (t_7)^2 t_1 t_2 t_6}{t_5} + J_2 (t_7)^2 + m (t_3 t_7)^2 - m t_4 t_6 (t_7)^2 t_3 \\
& - m \left(\frac{t_2 t_7 t_6}{t_5} \right)^2 - \frac{m t_4 t_3 t_6 (t_7)^2}{t_5} + \frac{m (t_4 t_6 t_7)^2}{t_5} + J_3 \left(\frac{t_6 t_7}{t_5} \right)^2.
\end{aligned}$$

5. FORMULATION OF HAMILTON'S EQUATIONS FROM THE BOND GRAPH

Hamiltonian equation is defined as:

$$H = \sum_i p_i \dot{q}_i - L, \quad (36)$$

where $i = 1, 2, 3, \dots, n$, p_i is the generalized momentum, and \dot{q}_i is the generalized velocity:

$$\dot{q}_i = \frac{\partial H}{\partial p_i}, \quad (37)$$

$$\dot{p}_i = -\frac{\partial H}{\partial q_i}. \quad (38)$$

Hamilton’s equation for dynamics can be obtained from the bond graph using the HaCAP procedure [12]. Hamilton’s equations are first-order equations in terms of state variables such as the generalized momentum of I -type elements and the generalized coordinates q .

For obtaining the Hamiltonian formulation from the bond graph of the quick return mechanism, integral causality has been assigned to I -element attached by bond 1, shown in Fig. 7. The Hamiltonian formulation can be derived based on causality propagation using global causality constraints [12]. Equations (39) and (40) are derived from the Hamiltonian bond graph shown in Fig. 7.

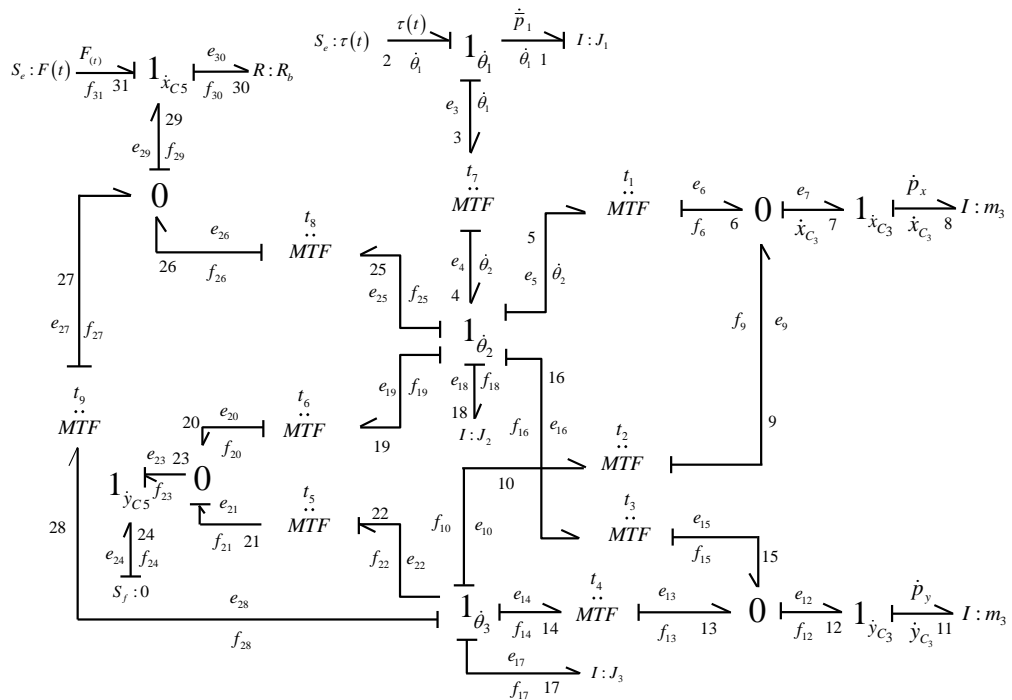


FIG. 7. Hamiltonian bond graph.

6. SIMULATION AND RESULTS

Both the bond graph models shown in Figs 6 and 7 have been simulated for a time span of 10 seconds using ode45 [15] solver in MATLAB. A constant torque $2 N \cdot m$ has been applied to the crank. The plots of various properties have been drawn and analyzed. The comparison between the various plots of the Lagrangian formulation of the second kind and Hamilton formulations has been conducted. The simulation time in MATLAB has been calculated in both cases. The numerical simulation time in the case of the Lagrangian formulation was 3.949503 seconds, while the Hamiltonian formulation took 3.856891 seconds.

6.1. The crank

The crank rotates about its origin O . Second end of the crank is attached to the slider 1 by a pin joint at point O_1 (shown in Fig. 1). The slider 1 slides in the slot of the rocker arm. During the rotation of the crank, the trajectory of the point O_1 is circular, shown in Fig. 8. Z -component will remain constant as the crank rotates about Z -axis.

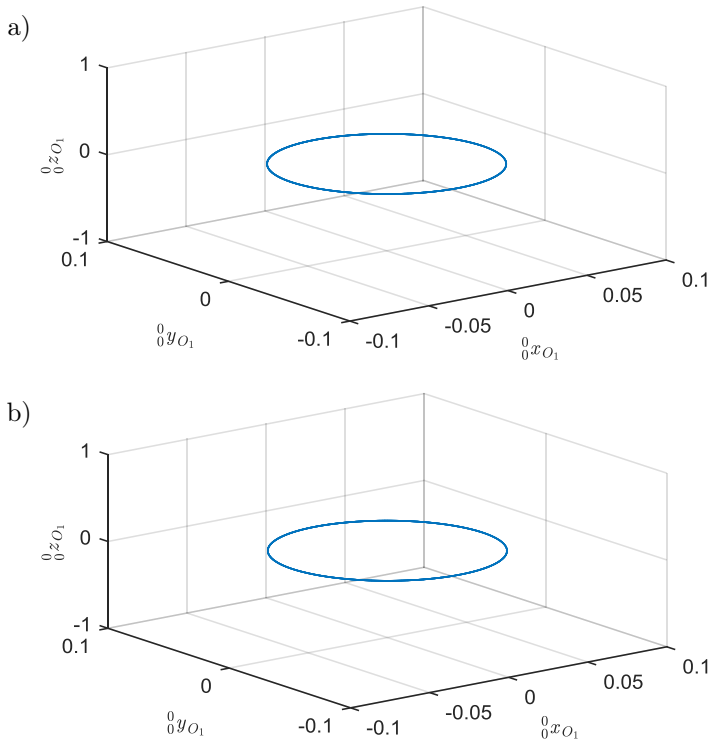


FIG. 8. The trajectory of the point O_1 with respect to time: a) Lagrangian case, b) Hamiltonian case.

The Hamilton equation of quick return mechanism:

$$\dot{p}_1 = \tau - (c^*)\ddot{q}_1 - (d^*)\dot{q}_1 + \left(\frac{t_9 t_7 t_6}{t_5} - t_7 t_8 \right) F, \tag{39}$$

where

$$c^* = m(t_1 t_7)^2 - \frac{m(t_7)^2 t_6 t_2 t_1}{t_5} + m(t_3 t_7)^2 - \frac{m(t_7)^2 t_4 t_6 t_3}{t_5} + J_2(t_7)^2 - \frac{m(t_7)^2 t_1 t_6 t_2}{t_5} + m \left(\frac{t_6 t_7 t_2}{t_5} \right)^2 - \frac{m(t_7)^2 t_4 t_6 t_3}{t_5} + m \left(\frac{t_6 t_7 t_4}{t_5} \right)^2 + J_3 \left(\frac{t_6 t_7}{t_5} \right)^2,$$

$$\begin{aligned}
 d^* = & mt_1 (t_7)^2 \dot{t}_1 + mt_7 (t_1)^2 \dot{t}_7 - \frac{mt_7 t_2 t_6 t_1}{t_5} \dot{t}_7 - \frac{m (t_7)^2 t_1 t_2}{t_5} \dot{t}_6 - \frac{m (t_7)^2 t_1 t_6}{t_5} \dot{t}_2 \\
 & + \frac{m (t_7)^2 t_1 t_6 t_2}{(t_5)^2} \dot{t}_5 + mt_7 (t_3)^2 \dot{t}_7 + mt_3 (t_7)^2 \dot{t}_3 - \frac{mt_4 t_6 t_7 t_3}{t_5} \dot{t}_7 \\
 & - \frac{m (t_7)^2 t_4 t_3}{t_5} \dot{t}_6 - \frac{m (t_7)^2 t_6 t_3}{t_5} \dot{t}_4 + \frac{m (t_7)^2 t_4 t_6 t_3}{(t_5)^2} \dot{t}_5 + J_2 t_7 \dot{t}_7 \\
 & - \frac{m (t_7)^2 t_6 t_2}{t_5} \dot{t}_1 - \frac{mt_7 t_2 t_6 t_1}{t_5} \dot{t}_7 + mt_7 \left(\frac{t_6 t_2}{t_5} \right)^2 \dot{t}_7 + mt_6 \left(\frac{t_2 t_7}{t_5} \right)^2 \dot{t}_6 \\
 & + mt_2 \left(\frac{t_6 t_7}{t_5} \right)^2 \dot{t}_2 - \frac{m (t_2 t_6 t_7)^2}{(t_5)^3} \dot{t}_5 - \frac{mt_3 t_4 t_7 t_6}{t_5} \dot{t}_7 - \frac{m (t_7)^2 t_4 t_6}{t_5} \dot{t}_3 \\
 & + mt_7 \left(\frac{t_6 t_4}{t_5} \right)^2 \dot{t}_7 + mt_6 \left(\frac{t_4 t_7}{t_5} \right)^2 \dot{t}_6 + mt_4 \left(\frac{t_6 t_7}{t_5} \right)^2 \dot{t}_4 - m \frac{(t_4 t_7 t_6)^2}{(t_5)^3} \dot{t}_5 \\
 & + J_3 t_7 \left(\frac{t_6}{t_5} \right)^2 \dot{t}_7 + J_3 t_6 \left(\frac{t_7}{t_5} \right)^2 \dot{t}_6 - J_3 \frac{(t_6 t_7)^2}{(t_5)^3} \dot{t}_5 + R \left(\frac{t_9 t_6 t_7}{t_5} \right)^2 \\
 & - 2R \frac{(t_7)^2 t_9 t_8 t_6}{t_5} + R (t_7 t_8)^2,
 \end{aligned}$$

$$\dot{q}_1 = \frac{p_1}{J_1}. \tag{40}$$

6.2. The rocker arm

The rocker arm oscillates about the origin O_2 . Relative to the movement of the crank, the angle θ_2 of the rocker arm increases and decreases due to the arm's oscillation. This variation of the angle θ_2 with respect to the angle θ_1 is shown in Fig. 9. The slope of the curve during the rotation from 0 to π radians is less than the slope of the curve during π to 2π radians. It is clear from the graph that this variation in the slope is due to the quick return mechanism of the system. The variation of the angular velocity of the rocker arm $\dot{\theta}_2$ with respect to the angle θ_1 has been shown in Fig. 10. The variation in the magnitude of the angle $\dot{\theta}_2$ during the forward stroke and backward stroke in Fig. 10 also validates the quick return mechanism of the system. The rocker arm oscillates about its origin O_2 . Relative to the movement of the rocker arm, the center of mass C_2 of the rocker arm traces a trajectory in an arc. This is shown in Fig. 11.

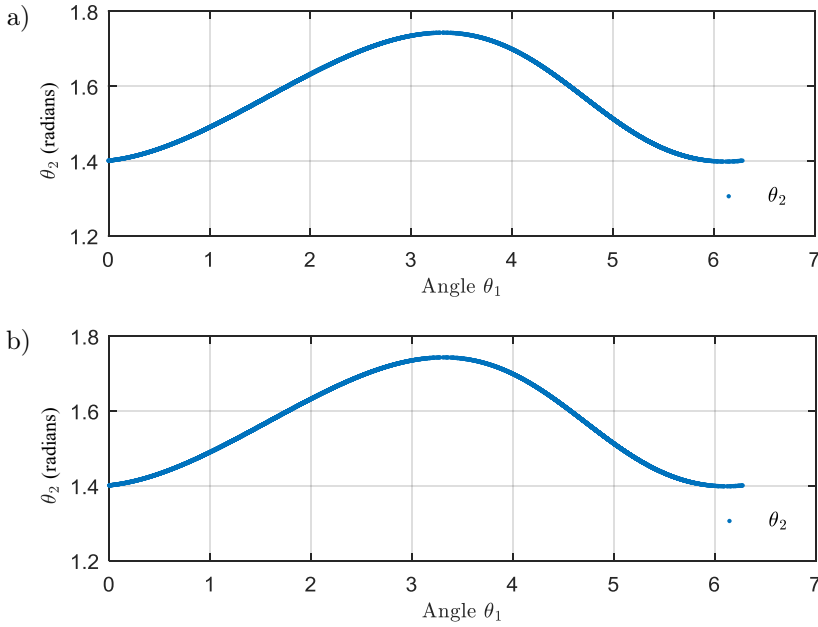


FIG. 9. Variation of the angle θ_2 of the rocker arm with respect to the angle θ_1 :
 a) Lagrangian case, b) Hamiltonian case.

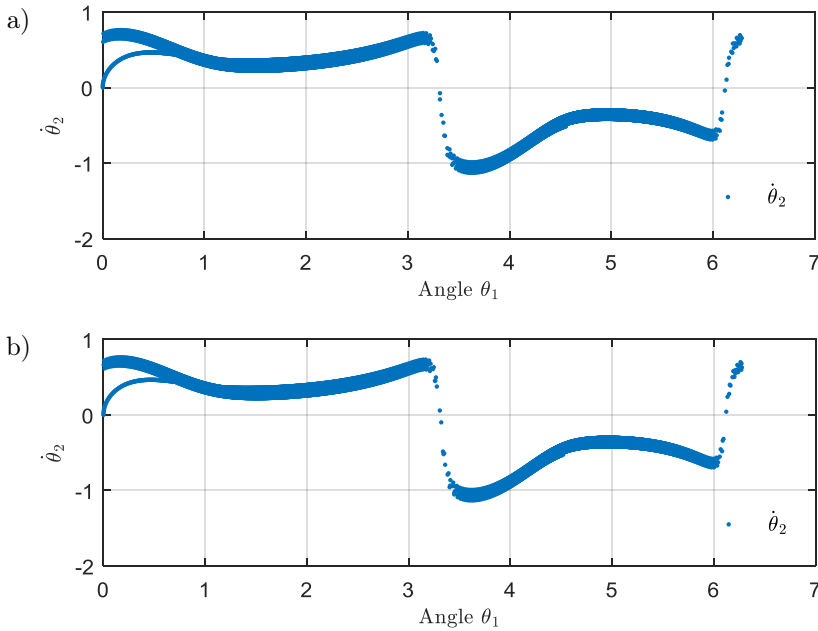


FIG. 10. Angular velocity $\dot{\theta}_2$ of the rocker arm with respect to the angle θ_1 :
 a) Lagrangian case, b) Hamiltonian case.

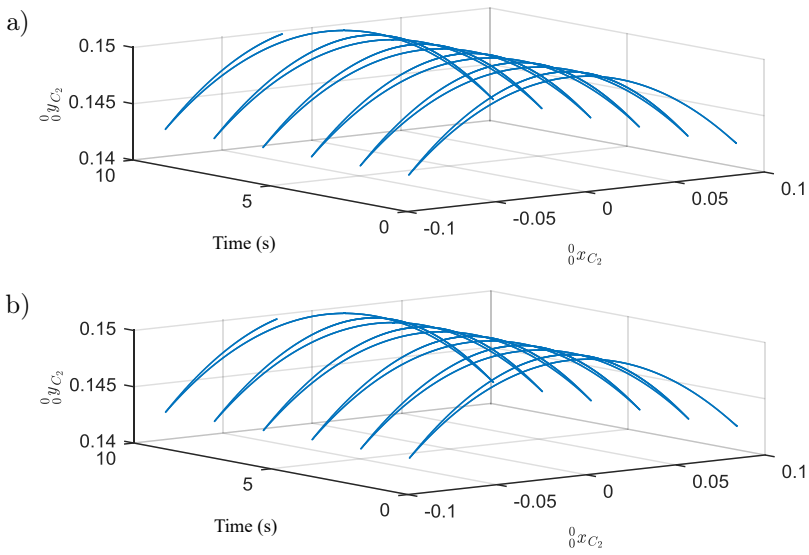


FIG. 11. Position of the center of mass C_2 of the rocker arm (link 2) *versus* time: a) Lagrangian case, b) Hamiltonian case.

6.3. The connecting rod

The angle between the rocker arm and the connecting rod is θ_3 . The variation in this angle with respect to the angle θ_1 is shown in Fig. 12. It is clear from

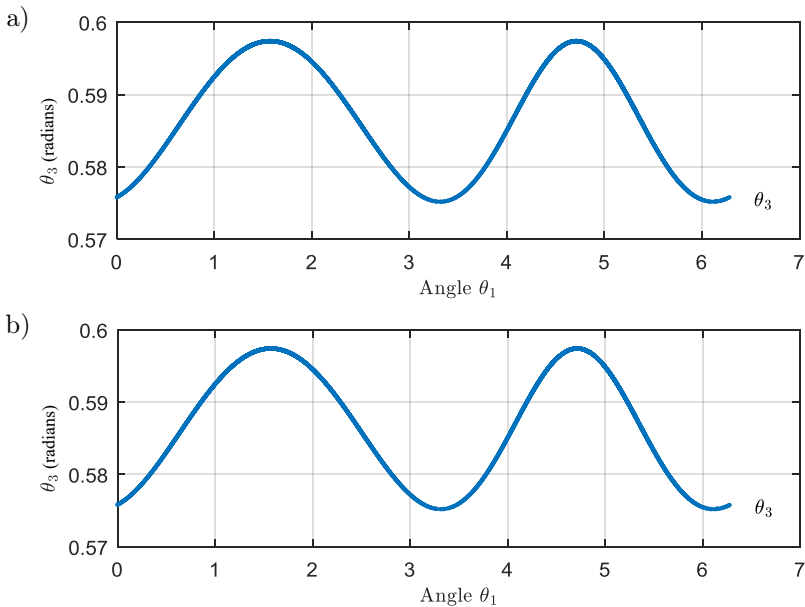


FIG. 12. Variation of the angle θ_3 of the connecting rod with respect to the crank angle: a) Lagrangian case, b) Hamiltonian case.

the graph that during one rotation of the crank, the connecting rod covers one forward stroke during the clockwise rotation of the crank from 0° to 180° (π^c) and one backward stroke during 180° (π^c) to 360° ($2\pi^c$). The variation of the

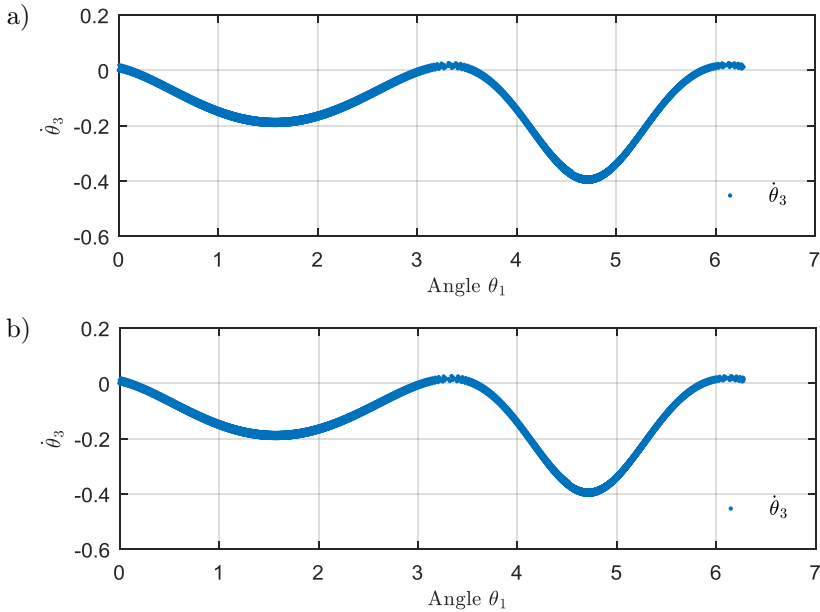


FIG. 13. Variation in angular velocity $\dot{\theta}_3$ of the rocker arm with respect to the angle θ_1 :
a) Lagrangian case, b) Hamiltonian case.

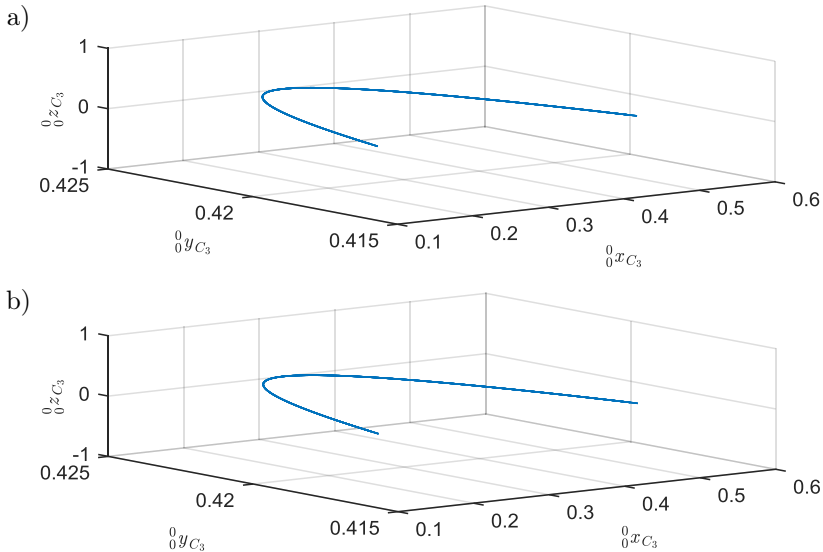


FIG. 14. The trajectory of the center of mass C_3 of the connecting rod:
a) Lagrangian case, b) Hamiltonian case.

angular velocity of the connecting rod $\dot{\theta}_3$ with respect to the rotation of the crank is shown in Fig. 13. The connecting rod oscillates about Z -axis. The path covered by the center of mass C_3 is curvilinear. The position of the center of mass of the connecting rod is shown in Fig. 14.

6.4. The slider 2

The movement of the slider 2 is permitted in one direction only. The slider 2 reciprocates in X -direction of the inertial frame only. The movement in the other two directions is constrained. The trajectory of the center of mass C_5 of the slider 2 is shown in Fig. 15. It is clear that Y and Z components are constants and only X component changes with respect to time.

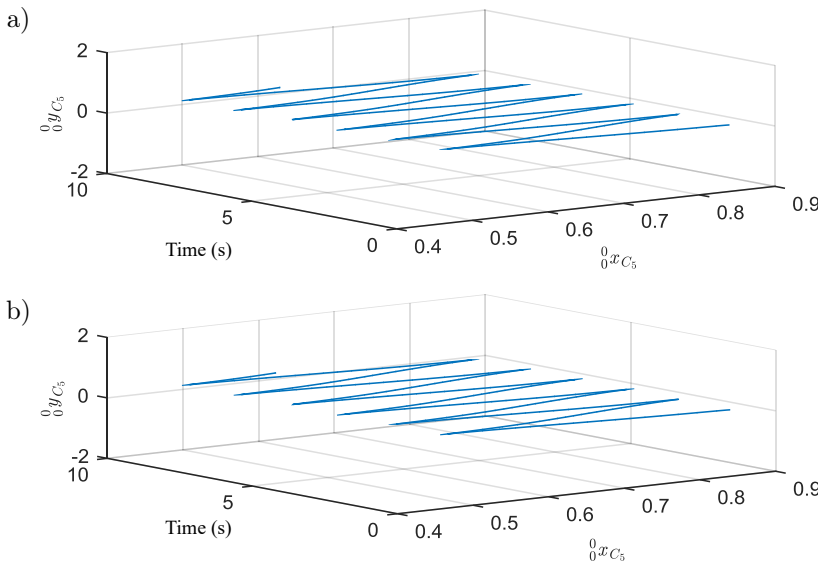


FIG. 15. Position of the center of mass C_5 with respect to time:
 a) Lagrangian case, b) Hamiltonian case.

The distance between the point O_1 at the slider 1 and O_2 at the origin of the rocker arm is L_x . The length L_x varies due to the oscillating movement of the slider 1. The slider 1 slides with the rotation of the crank. The variation in L_x versus time is shown in Fig. 16. Figure 17 shows the variation in the angular momentum of the crank, the rocker arm, and the connecting rod with respect to the angle θ_1 . It is clear from Fig. 17 that the angular momentum ${}^0_{C_1}z_{p_1}$ of the crank with respect to its center of mass changes slightly during the rotation of crank from 0° to 180° (π^c) and 180° (π^c) to 360° ($2\pi^c$).

The rocker arm oscillates about its origin. During the one rotation of the crank, it covers two strokes, one in the forward direction and another in the back-

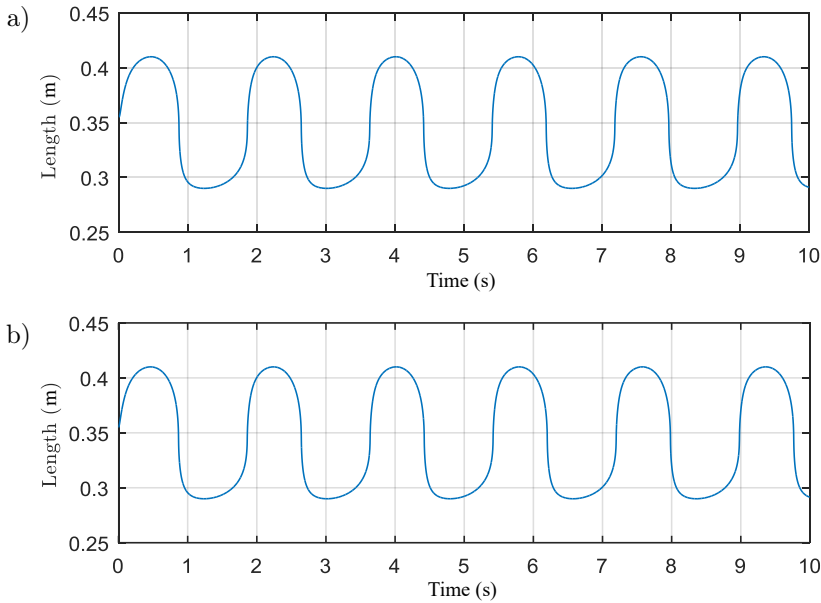


FIG. 16. Variation of length L_x versus time: a) Lagrangian case, b) Hamiltonian case.

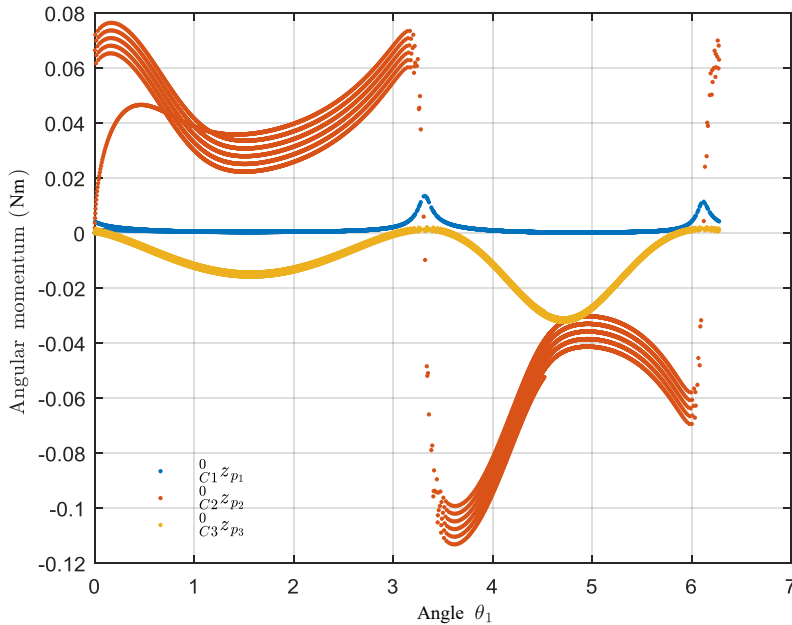


FIG. 17. Variation in the angular momentum of the crank, the rocker arm, and the connecting rod versus the angle θ_1 (Hamiltonian case).

ward direction. During the backward direction, 180° (π^c) to 360° ($2\pi^c$) rotation of the crank, the speed of the rocker arm will be more than the speed in the forward

stroke from 0° to 180° (π^c) due to the quick return mechanism of the system. So the magnitude of the angular momentum ${}^0_{C_2}z_{p_2}$ acting on the rocker arm will be more during backward stroke than the forward stroke. This is clear from Fig. 17.

The connecting rod oscillates and transmits the movement to the slider 1. The angular momentum ${}^0_{C_3}z_{p_3}$ of the connecting rod is more in the backward stroke 180° (π^c) to 360° ($2\pi^c$). The plot showing the variation in the angular momentum ${}^0_{C_3}z_{p_3}$ of the connecting rod satisfies the condition. The rotation of the crank, the rocker arm, and the connecting rod is about Z -axis, so there will be no variation in the angular momentum in X -direction and Y -direction. Only the variation in the angular momentum about Z -direction has been plotted.

The above plots shown in Figs 8–16 represent the various kinematic properties of the various links for both cases: Lagrangian and Hamiltonian formulation. The analysis and comparison show that the plots obtained from both aforementioned formulations agree with each other.

The Lagrangian form gives the ODE in the terms of generalized displacement q_1 and its time derivative \dot{q}_1 generalized velocity while the Hamiltonian equations are in terms of generalized displacement q_1 and generalized momentum p_1 . So, Fig. 17 shows the variation of the angular momentum acting on the various links in the Hamiltonian case only.

7. CONCLUSIONS

This paper shows the use of alternative causality assignment procedures to derive different dynamic formulations for the quick return mechanism. The concept of causality, elegantly represented in the bond graph, was used and the equations of dynamics were written by following the causal paths. By adopting these alternative causality assignment procedures, Lagrange's equations of the first kind with the λ multiplier, Lagrange's equations of the second kind, and Hamilton's equations of motion of the quick return mechanism were derived from the bond graph. Simulation was carried out using ode45 solver in MATLAB. It was shown that numerical simulation results obtained from the aforementioned formulations agree with each other.

REFERENCES

1. F.T. Brown, Lagrangian bond graphs, *Journal of Dynamic Systems, Measurement, and Control*, **94**(3): 213–221, 1972.
2. R.M. Murray, Z. Li, S.S. Sastry, *A Mathematical Introduction to Robotic Manipulation*, CRC Press, 1994.
3. H. Goldstein, *Classical Mechanics, Second Edition*, Narosa Publishing House, 1998.

4. F.T. Brown, Bond graphs for nonholonomic dynamic systems, *Journal of Dynamic, Measurement, and Control*, **98**(4): 361–366, 1976, doi: 10.1115/1.3427052.
5. D. Karnopp, Understanding multibody dynamics using bond graph representations, *Journal of the Franklin Institute*, **334**(4): 631–642, 1997, doi: 10.1016/S0016-0032(96)00083-X.
6. A. Mukherjee, R. Karmarkar, *Modelling and Simulation of Engineering Systems through Bondgraphs*, Narosa Publishing House, 2000.
7. D.C. Karnopp, D.L. Margolis, R.C. Rosenberg, *System Dynamics: Modeling and Simulation of Mechatronic Systems*, John Wiley & Sons Inc., 2012.
8. A. Mukherjee, R. Karmarkar, A.K. Samantaray, *Bond Graph in Modeling, Simulation and Fault Identification*, I.K. International Publishing House Pvt. Ltd, 2006.
9. D.C. Karnopp, D. Margolis, R.C. Rosenberg, *System Dynamics: Modeling and Simulation of Mechatronic Systems*, New York: Wiley-Interscience, 2006.
10. W. Borutzky, *Bondgraph Methodology: Development and Analysis of Multidisciplinary Dynamic System Models*, London: Springer-Verlag, 2010.
11. R. Merzouki, A.K. Samantaray, P.M. Pathak, B.O. Bouamama, *Intelligent Mechatronic Systems: Modeling, Control and Diagnosis*, London: Springer-Verlag, 2013, doi: 10.1007/978-1-4471-4628-5.
12. W. Marquis-Favre, S. Scavarda, Alternative causality assignment procedures in bond graph for mechanical systems, *Journal of Dynamic Systems, Measurement, and Control*, **124**(3): 457–463, 2002.
13. D. Karnopp, Lagrange's equations for complex bond graph systems, *Journal of Dynamic Systems, Measurement, and Control*, **99**(4): 300–306, 1977, doi: 10.1115/1.3427123.
14. F.T. Brown, Hamiltonian and Lagrangian bond graphs, *Journal of the Franklin Institute*, **328**(5–6): 809–831, 1991.
15. L.F. Shampine, M.W. Reichelt, The MATLAB ODE Suite, *SIAM Journal on Scientific Computing*, **18**(1): 1–22, 1997.

Received June 25, 2020; revised version August 1, 2020.